

Electronic Supplementary Material

Effect of oxygen and nitrogen functionalization on the physical and electronic structure of graphene

Alexander J. Marsden¹, Peter Brommer^{1,2}, James J. Mudd¹, M. Adam Dyson¹, Robert Cook¹, María Asensio³, Jose Avila³, Ana Levy³, Jeremy Sloan¹, David Quigley^{1,2}, Gavin R. Bell¹, and Neil R. Wilson¹ (✉)

¹ Department of Physics, University of Warwick, Coventry, UK

² Centre for Scientific Computing, University of Warwick, Coventry, UK

³ Synchrotron SOLEIL, L'Orme des Merisiers, Saint Aubin-BP 48, 91192 Gif sur Yvette Cedex, France

Supporting information to DOI 10.1007/s12274-015-0768-0

1 CVD of graphene

Graphene was grown on low-cost copper foils (99.5% purity, 0.025 mm thick, Alfa Aesar product number 46365) using low pressure chemical vapour deposition. The foils were cleaned by electropolishing (10 s at 5 V, ~1.5 A) in an electrolyte containing orthophosphoric acid and urea, followed by rinsing in acetone and isopropanol. The growth was conducted inside a 1 inch diameter quartz tube under vacuum (10^{-1} mbar) with 20 sccm hydrogen flowing throughout. After 20 min annealing at 1,000 °C, 2 sccm methane was introduced for 10 min. The methane was kept on while the sample cooled to 600 °C, after which the flow was stopped.

Basic characterization is shown in Fig. S1 below. SEM, df-TEM and Raman spectroscopy are all consistent with the sample consisting of predominantly monolayer graphene. The df-TEM shows that the typical graphene grain size is ~5 μm . The large background in the Raman spectra is due to the copper foil; the relative intensities of the 2D and G, their narrow width, and the fact that they can be well fit by single Lorentzians, are all consistent with monolayer graphene. For the pristine graphene, no D peak is found.

Address correspondence to Neil.Wilson@warwick.ac.uk

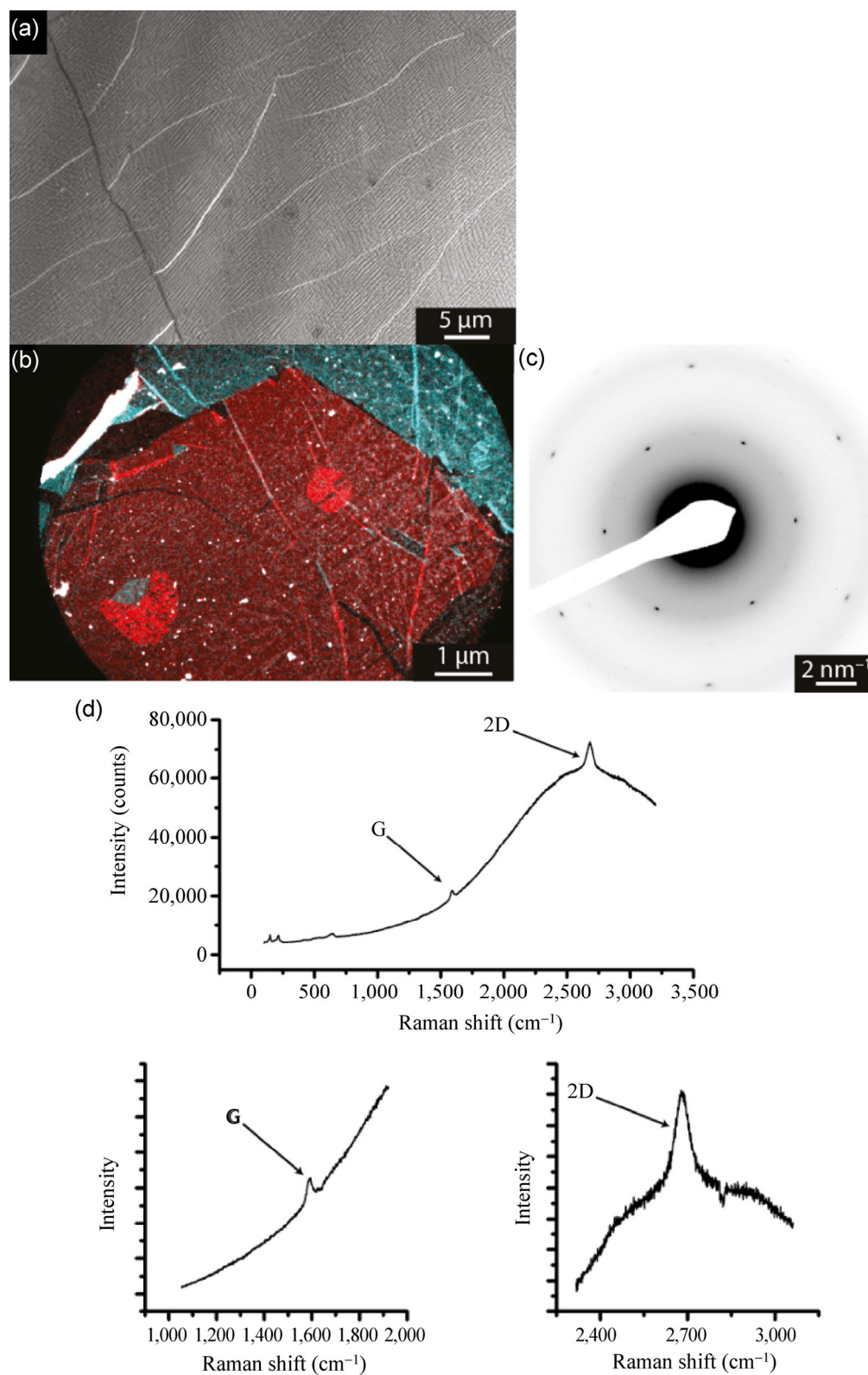


Figure S1 Characterization of as-grown graphene on copper. (a) SEM image, showing pale cracks in the graphene as well as darker wrinkles and bilayers; (b) darkfield TEM image, demonstrating the $> 5 \mu\text{m}$ graphene grain size and the preferred orientations; (c) shows a diffraction pattern from the red region in (b), the inner spots are more intense than the outer spots indicating single layer graphene; (d) typical Raman spectra from the pristine graphene whilst on the copper foil.

2 Atom sources

Atomic species were produced in UHV using a Gen 2 microwave plasma source (Tetra GmbH) in atom source mode. In this configuration apertures inhibit ions leaving the plasma, yielding mostly thermalized neutral species which do not damage the substrate. Oxygen or nitrogen gas was leaked through the source at a pressure of 5×10^{-5} mbar (base pressure 10^{-9}), after which the generator was set to 25 mA for the duration of each dose. For some of the Raman experiments on O-dosed graphene, we also used a thermal atom source (Oxford Applied Research Ltd.) in order to minimize atmospheric exposure time between functionalization and measurement. This is described in section 6. XPS measurements (not shown) indicated that the functionalization proceeded in a similar fashion for both atom sources.

3 Further XPS characterization of atomic oxygen dosed graphene

Figure S2 shows XPS of the O 1s region after dosing with atomic oxygen. The clean graphene exhibits some residual oxygen, even after annealing to 200 °C for 2 h. The majority of this oxygen is believed to be associated with oxidized copper (blue peak here) [S1]. Although the copper surface is almost fully coated with graphene,

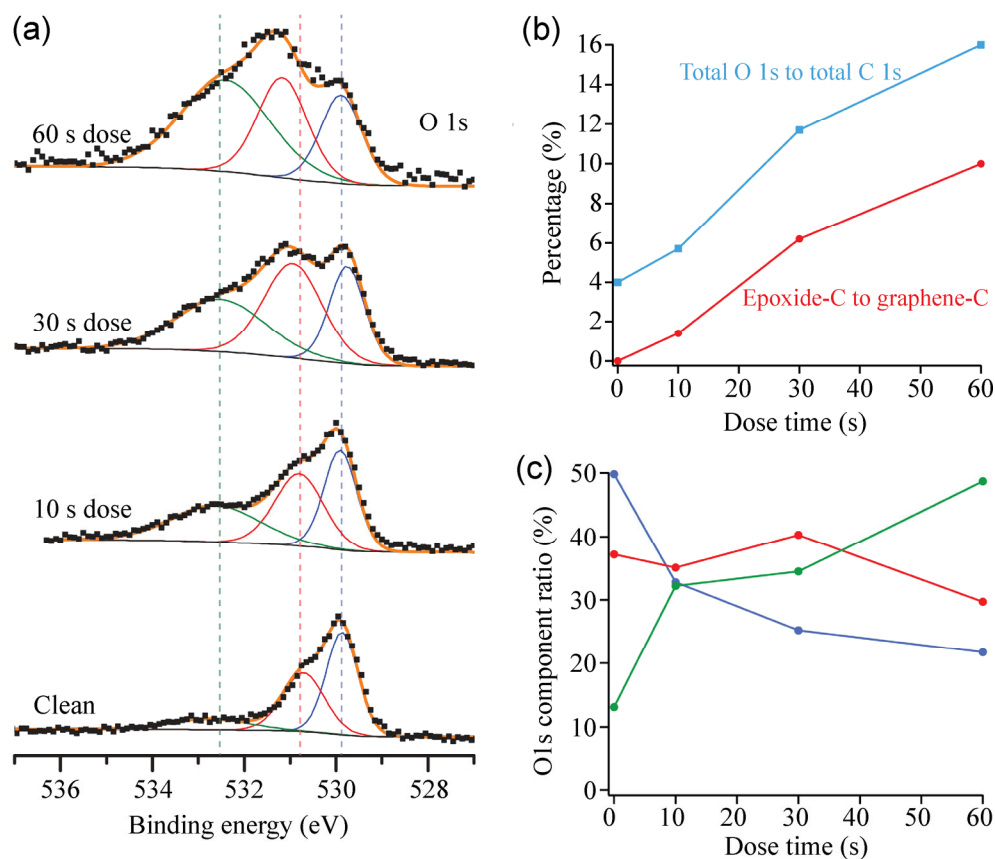


Figure S2 Further XPS from the O-dosed samples. (a) Shows the O 1s after different oxygen exposures. (b) Changes in the amount of oxygen compared to carbon during dosing measured in two ways: the first based on the formation of an epoxide peak on the shoulder of the C 1s (red, as shown in the main text); the second by measuring the total intensity in the C 1s and in the O 1s and correcting for sensitivity. (c) Changes in the individual components of the O 1s, colours as marked in (1).

there are inevitably small cracks and regions where the copper is exposed and has oxidized. The peaks at higher binding energy are often associated with C–O environments and here are possibly due to strongly adsorbed hydrocarbons in these regions as well. There is no evidence that any of this oxygen is bound to graphene, and the absence of a D peak in Raman spectra (as well as other experimental investigations such as scanning tunneling microscopy (STM) of these samples strongly suggests that this oxygen is not bound to graphene. This is consistent with the DoniachSunjichlineshape of the C 1s, with no other peaks evident, for pristine graphene.

Upon exposure to atomic oxygen, there is a clear increase in the peak at 532.8 eV; this strongly correlates to the increase in the “epoxy” peak in the C 1s. The O 1s also shows a smaller increase in the peak at 530.7 eV, but it is not clear to what extent this is due to changes in the copper oxide in the exposed areas of the sample. Certainly no corresponding increase in C=O can be seen in the C 1s spectra (this would be seen at 287.8 eV in the C 1s [S2], and given the signal to noise in that spectra would be clearly resolved).

Part (b) of Fig. S2 shows the ratio total intensity of the O 1s / total intensity of the C 1s as well as the ratio of epoxide-C: graphene-C that is shown in the main text. There is a strong correlation between them which supports the assignment of the “epoxide peak” in the C 1s to an oxygen containing group. Figure S2 (c) shows the changes in the individual components of the O 1s. Here, the only component that shows a consistent increase during dosing is that assigned to the epoxide environment (green).

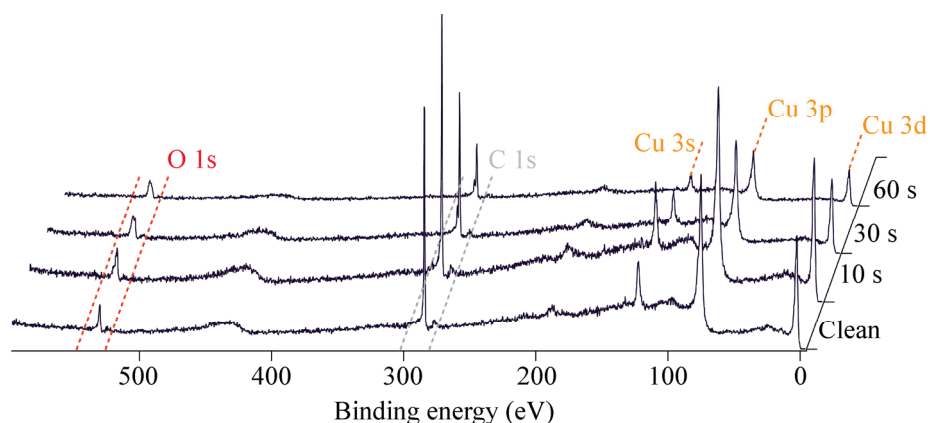


Figure S3 XPS survey scan showing the evolution of composition of graphene on copper upon exposure to atomic oxygen.

Scanning photoemission microscopy (SPEM) was used to identify the homogeneity of the O functionalisation on the sample. Figure S4 shows the SPEM maps of a graphene on copper sample that has been dosed with 30 s of oxygen. The averaged spectrum is shown in part (a) and the maps formed by integrating the regions are shown around the outside. The two regions mapped are roughly associated with O–C (high binding energy) and O–Cu (low binding energy) bonding. There is very little contrast in all of these images suggesting that, on these length scales, the functionalisation is uniform.

Once the dosing was complete the graphene on copper foils were annealed in UHV at 200 °C for 12 h. XPS before and after exposure, and after subsequent annealing, is shown in Fig. S5. Here the annealing removes nearly all of the epoxide groups, in agreement with Hossain et al. [S3].

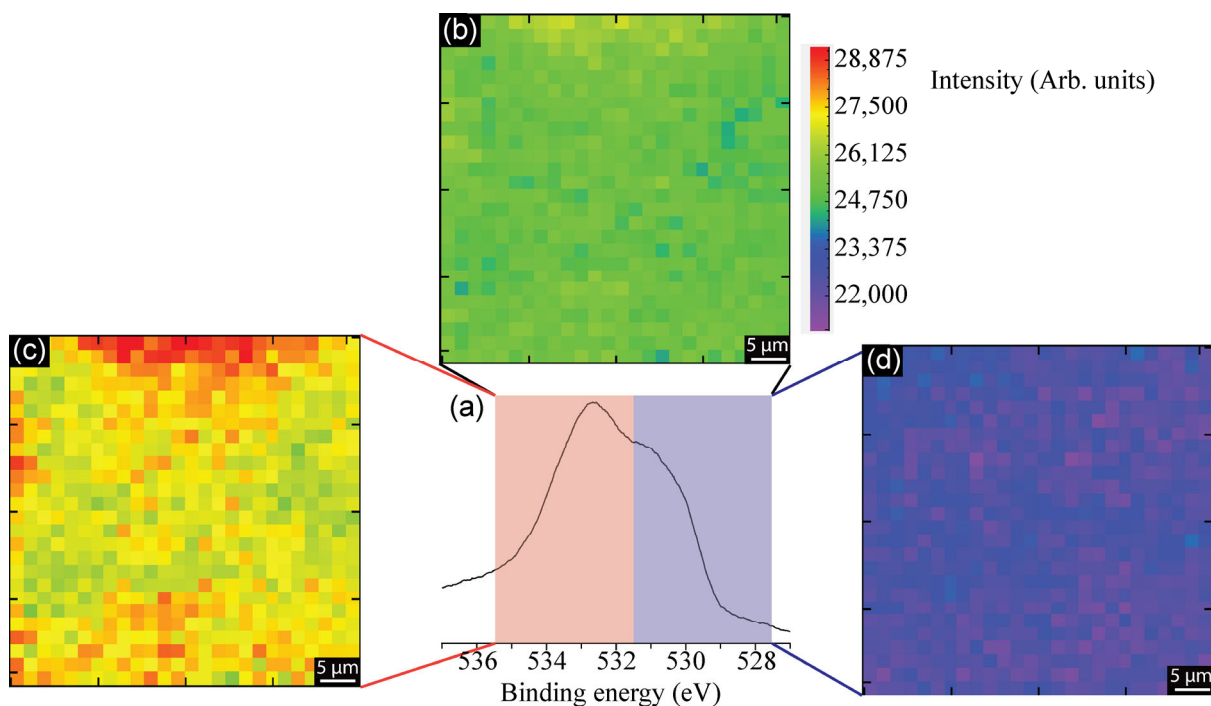


Figure S4 Scanning photoemission microscopy (SPEM) of O-dosed graphene on copper. Each coloured pixel represents an XPS spectrum and the average spectrum is shown in (a). Integrating over the combined red and blue regions gives the map in (b), while the red only (associated with oxygen on carbon) is shown in (c) and the blue (associated with oxygen on copper) only is shown in (d).

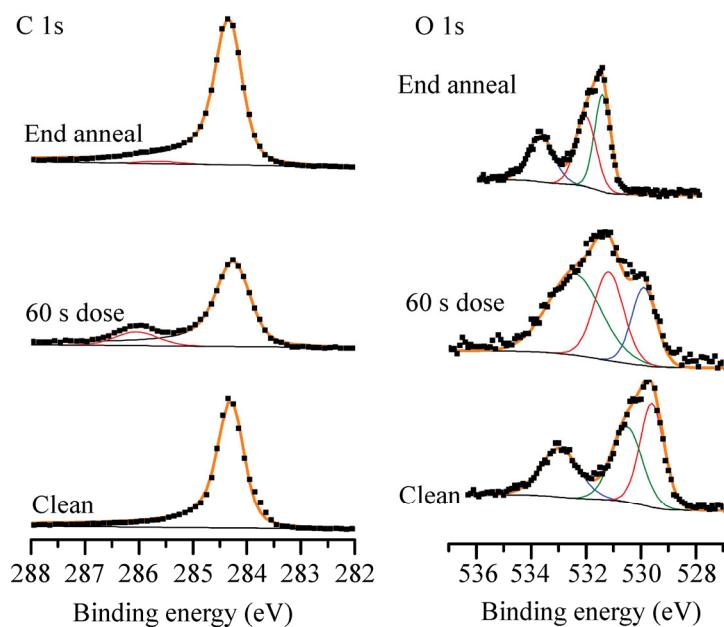


Figure S5 XPS region scans of the C 1s and the O 1s for clean graphene, a 60 s dose of atomic O and after annealing the dosed sample at 200 °C for 12 h.

4 acTEM of atomic oxygen dosed graphene

Figure S6 shows acTEM of a graphene sample after exposure to 30s of atomic oxygen. At the top of the region highlighted by the dashed white box there is a bright feature on the graphene lattice. Using Fourier filtering to remove the graphene contrast (shown in (b)) reveals a circular region of brighter contrast. An exit wave simulation of an epoxide group is shown in part (c), comparison between the simulation and experimental image suggests that the bright feature could be due to an adatom like an oxygen epoxide group. Similar features were not observed on pristine graphene and these features did not remain stationary long enough to acquire a focal series.

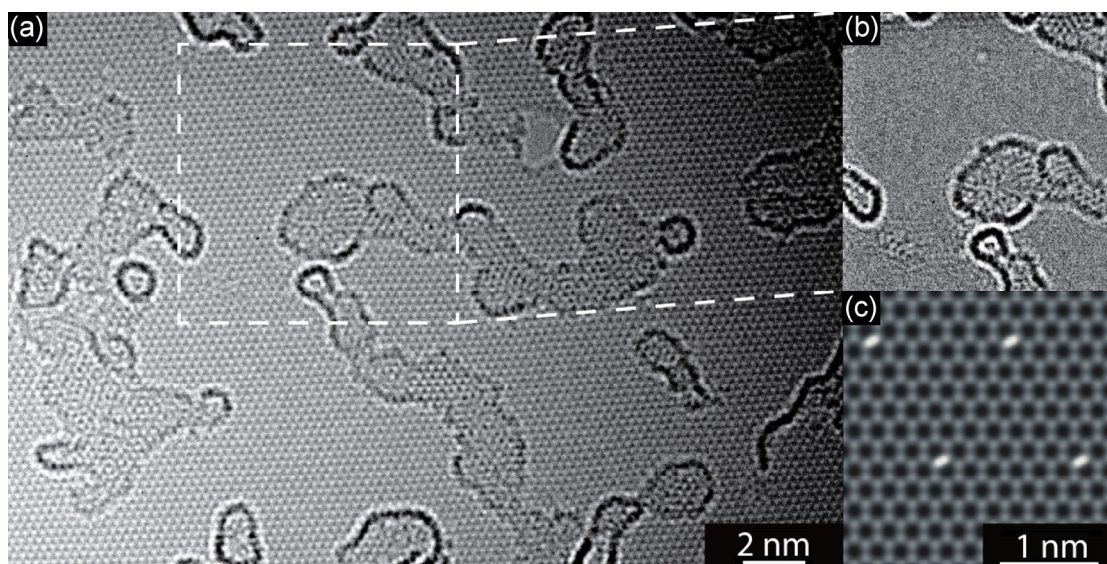


Figure S6 acTEM of O-dosed graphene. (a) is the raw image of graphene dosed with 30 s of O. (b) shows a Fourier filtered region highlighted by the dashed line. By removing the contrast from the graphene lattice, the feature is easier to see, which is possibly an epoxide group attached to the graphene surface. (c) shows an exit-wave simulation of an epoxide group on the graphene surface.

5 Further XPS characterization of atomic nitrogen dosed graphene

Figure S7 shows survey scans of graphene on copper before and after dosing with atomic nitrogen. A photon energy of 700 eV was used.

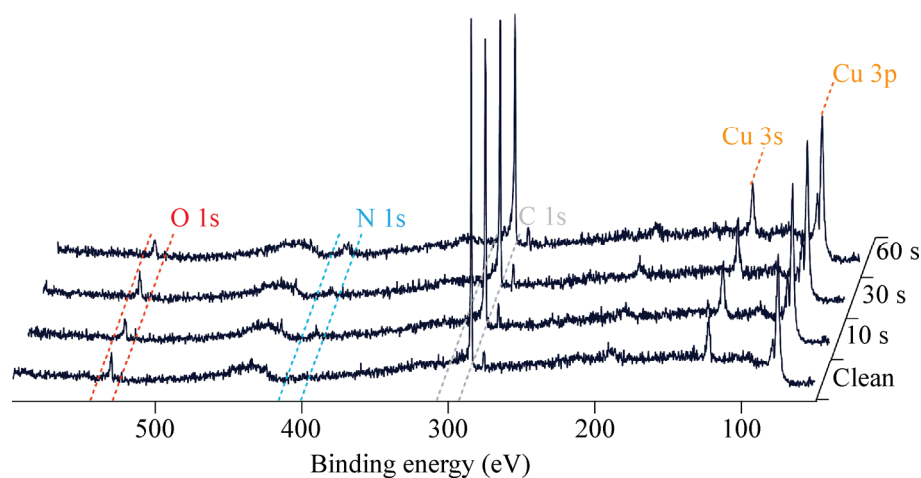


Figure S7 XPS survey scans before and after exposure of graphene on copper to atomic nitrogen.

Just as for the oxygen dosing, the nitrogen dosed graphene on copper foils were annealed in UHV at 200 °C for 12 h. Figure S8 shows XPS before and after exposure to atomic nitrogen, and after subsequent annealing. Unlike the oxygen dosed graphene, the annealing had little effect on the total nitrogen content, suggesting the nitrogen functionalisation is much less reversible. However, the intensities of the different peaks within the N 1s region do change. The peak assigned to the N adatom disappears after annealing, and the peak assigned to substitutional nitrogen grows relative to the pyridinic/pyrrolic nitrogen.

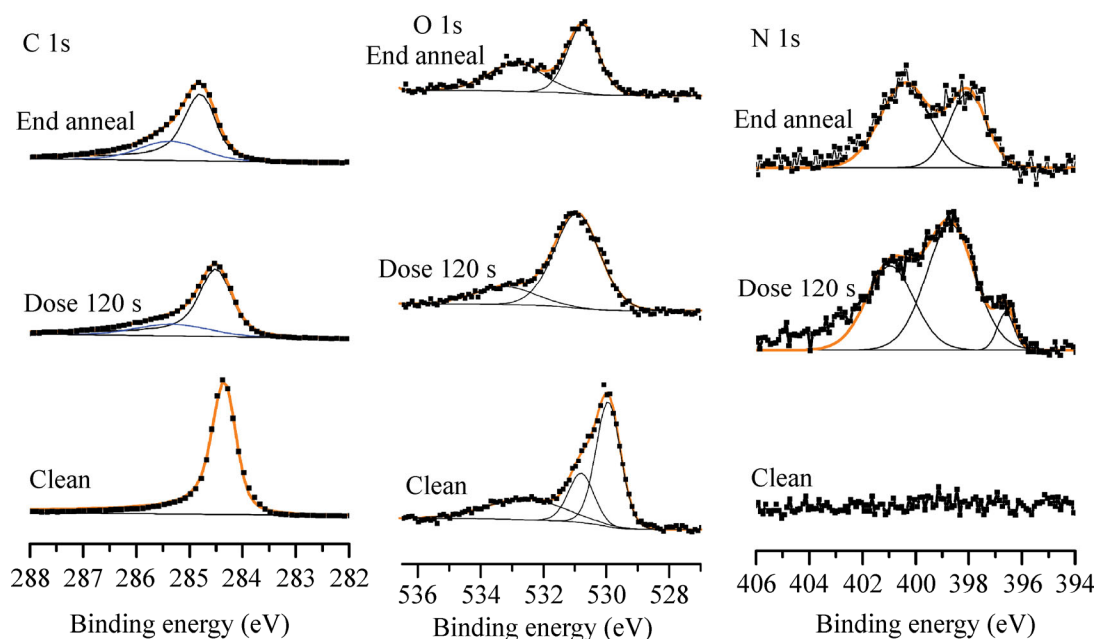


Figure S8 XPS regions scans for clean graphene, after a 120 s dose of atomic N and finally, after the foils were annealed at 200 °C for 12 h.

6 Raman of nitrogen and oxygen dosed graphene

Changes in the Raman spectra after exposure to atomic sources are shown in Fig. S9. The spectra were taken using a Renishaw inVia Raman microscope with 514.5 nm excitation. Pristine graphene shows a single sharp G peak with no evidence for a D peak. Upon exposure to atomic nitrogen, a D peak appears. Initially the D peak is sharp, but it broadens as the exposure time increases. A D' peak also appears after exposure to atomic nitrogen and grows with exposure time until it merges with the now broadened G peak to form a single asymmetric, broad peak.

We found that low levels of oxygen functionalization were unstable with exposure to atmosphere. In order to investigate the Raman signature of atomic oxygen exposed graphene on copper, we dosed using a high efficiency thermal cracker in a UHV chamber more local to the Raman spectrometer. XPS showed that the 60 s exposure with this source gave a higher epoxy carbon fraction than the RF cracker used for the results in the main text. Hence the 60 s thermal O exposed sample had a higher level of functionalization than the 120 s atomic N exposed sample. Despite this, the changes to the Raman spectrum are less profound. The G peak is still narrow, a significant but narrow D peak is present, and only a weak D' peak is evident. For both atomic oxygen and atomic nitrogen exposed graphene, the 2D peak rapidly reduced in intensity and broadened (results not shown).

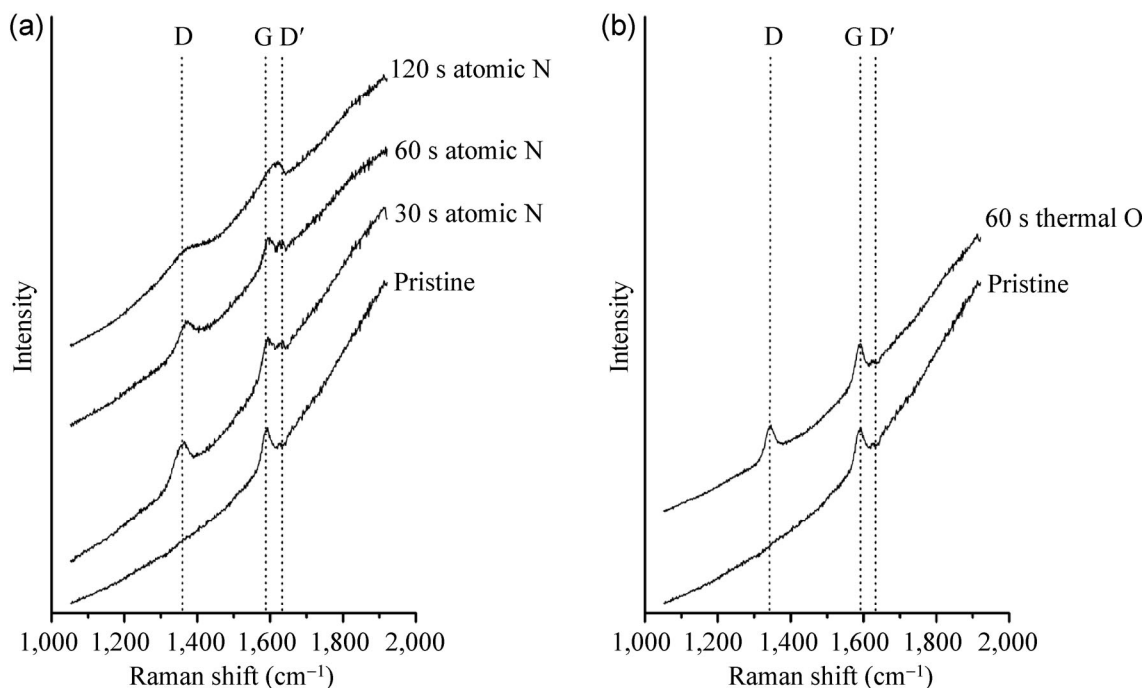


Figure S9 Raman spectra, centred on the D/G region, of pristine graphene on copper and after exposure to (a) atomic nitrogen and (b) atomic oxygen.

The Raman spectra are thus consistent with the XPS and acTEM results presented in the main text. Nitrogen dosing introduces a range of functional groups, including vacancies and extended topological defects. These broaden the peaks and induce a significant D'. By contrast, the atomic oxygen introduces epoxy groups, and as these functional groups are less perturbing of the graphene lattice their effect on the Raman spectra is less pronounced.

7 Fitting ARPES data to extract $E_D - E_F$

Figure S10 illustrates how the shift in the Dirac point energy (E_D) relative to the Fermi energy (E_F) is extracted from ARPES data. Extracting this requires ARPES data taken in both angular directions because, for graphene, intensity beyond the K-point in the Γ -K direction is lost due to selection rules. As a result, a slice through the Dirac point in the Γ -K direction shows only one side of the Dirac cone meaning that the top of the cone cannot easily be found by just looking at the maxima in orthogonal slices. In order to unambiguously find the top of the Dirac cone we fit momentum distribution curves (MDCs, at constant energy) taken from cuts through the three-dimensional dataset perpendicular to the Γ -K direction, as shown in Fig. S10. From this cut, Lorentzian peaks were fit to the MDCs to find the linear dispersion of the bands; these coordinates are shown by the blue lines in the main panel. The bands were only fit where they are distinguishable from each other. These lines were then extrapolated (black lines) to where they crossed. Taking a cut across the Dirac cone at any point other than the K-point will give a crossing at an energy lower than the Dirac point. To find $E_D - E_F$, the procedure was repeated at successive slices until the intensity of the bands had disappeared. The maximum value of E_D is taken as the true Dirac point, and the correct measure of the doping. The difference in energy between this Dirac point and the Fermi level gives the doping of graphene, as discussed in the main text.

Note that the ARPES data here and in the main text has been shown as a function of the collection angles rather than as a function of the electron momentum. The copper foil was not perfectly flat, as a result the Γ point (i.e., the surface normal) was not exactly aligned with the zero points of the collection angles (see schematic in Fig. 1

of the main text). This complicates transforming from the collection angles to the two-dimensional momentum vector. As the analysis here was focused on extracting the energy at the Dirac point and did not involve quantitative analysis of the band dispersion, the data was not transformed. Approximate transformations were applied to cuts of the Dirac cones to check that the Fermi velocity was consistent with our previous reports [S4, S5].

As with our previous reports [S4, S5], we found that the pristine graphene on copper was undoped after mild thermal annealing which, as discussed above, does not remove all residual oxygen. The copper foils used here after growth show predominantly near Cu(001) grains. We note that other reports that have looked at CVD graphene on Cu(111) have found it to be n-doped after annealing at slightly higher temperatures which result in lower levels of residual oxygen [S6, S7]. However, the C1s XPS lineshape and the absence of a D peak in the Raman spectroscopy measurements for pristine graphene both demonstrate that the residual oxygen is not covalently bound to the graphene and so does not interfere with the subsequent oxygen functionalization measurements reported here. The difference in doping between the different measurements of pristine graphene is likely due to the differences in copper surface crystallography.

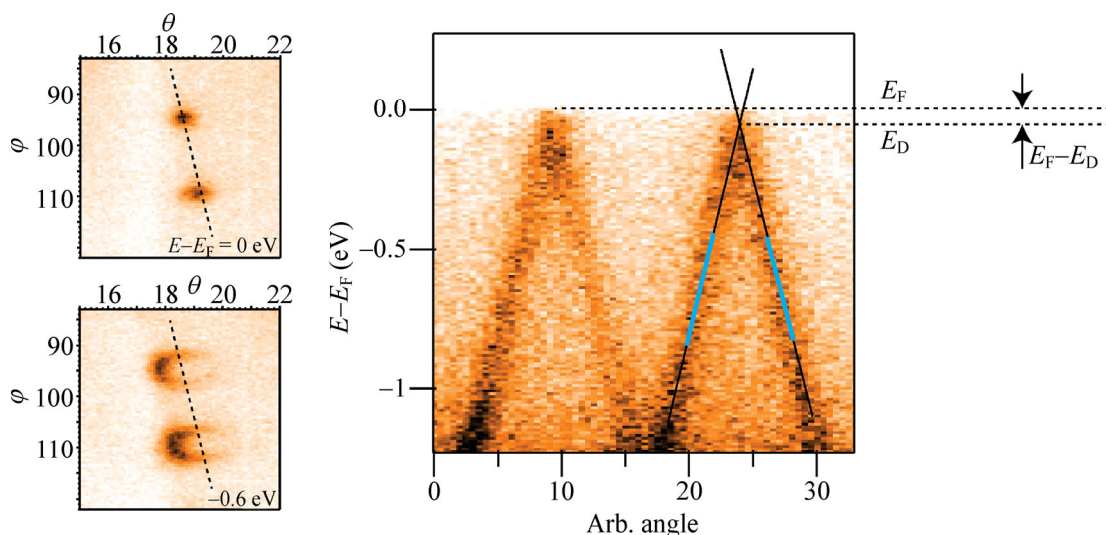


Figure S10 Left, constant energy slices through two Dirac cones at the Fermi energy and 0.6 eV below it. In the latter, the asymmetry in the ARPES signal due to the selection rules is clear. The dashed lines indicate the direction of the slice shown on the right. On it are marked the fits to one of the Dirac cones.

8 Band structure calculations and extraction of $E_D - E_F$ from calculated band structures

Defect structures and band structures were determined in a 6×6 supercell containing 69–72 carbon atoms and 1 nitrogen or oxygen atom, equating to a dopant concentration of approximately 1.4%. A standard band structure of such a supercell would not be useful, as all bands get folded into the first Brillouin zone of the supercell, whose reciprocal volume is only 1/36 compared to the graphene primitive cell. This would result in an extremely crowded picture. To extract any meaningful information from this calculation, the band structure was unfolded using a recently implemented add-on to CASTEP. This process yields an effective band structure (EBS), which is discontinuous in band energy. The EBS quantifies how a supercell band contributes at a certain reciprocal lattice point in the primitive cell. In this way, it provides an interpretation of the electronic structure using the same k-space description as the ARPES uses.

To directly compare the calculated band structures to the experimental data, we calculate the effective Dirac point energy shift relative to the Fermi energy from the band structure at the K point. The optimized structures, and effective band structures, for the functional groups discussed in the main paper are shown in Figs. S11 and

S12 below. The band structures are shown as histograms plotted to the right in arbitrary units for each k point the band structure was evaluated at. The vertical base line for each histogram is suppressed where there is no significant contribution to the band density. Note that many other possible positions for the nitrogen atoms were investigated, but the ones shown are the lowest energy arrangements found (subject to the constraint of only one nitrogen per supercell). Each of the band structures plotted in Figs. S11 and S12 correspond to a periodically repeating array of defect/adatom motifs, sufficiently separated to be effectively isolated. To a first approximation (neglecting interactions between motifs) the band structure of a disordered sample can be considered a superposition of these plots, weighted by energy and composition as appropriate to the thermal and chemical environment. This is shown in Fig. S13 and demonstrates broadening and slight overall p-doping, under the assumption that only one nitrogen is associated with each vacancy and that the pyridinic and pyrrolic nitrogen are present in equal proportion. The individual band structures plotted in Figs. S11 and S12 cannot directly compared to the experimental ARPES results, but they do serve as a useful guide for interpreting the evolution of bandstructure with functionalization.

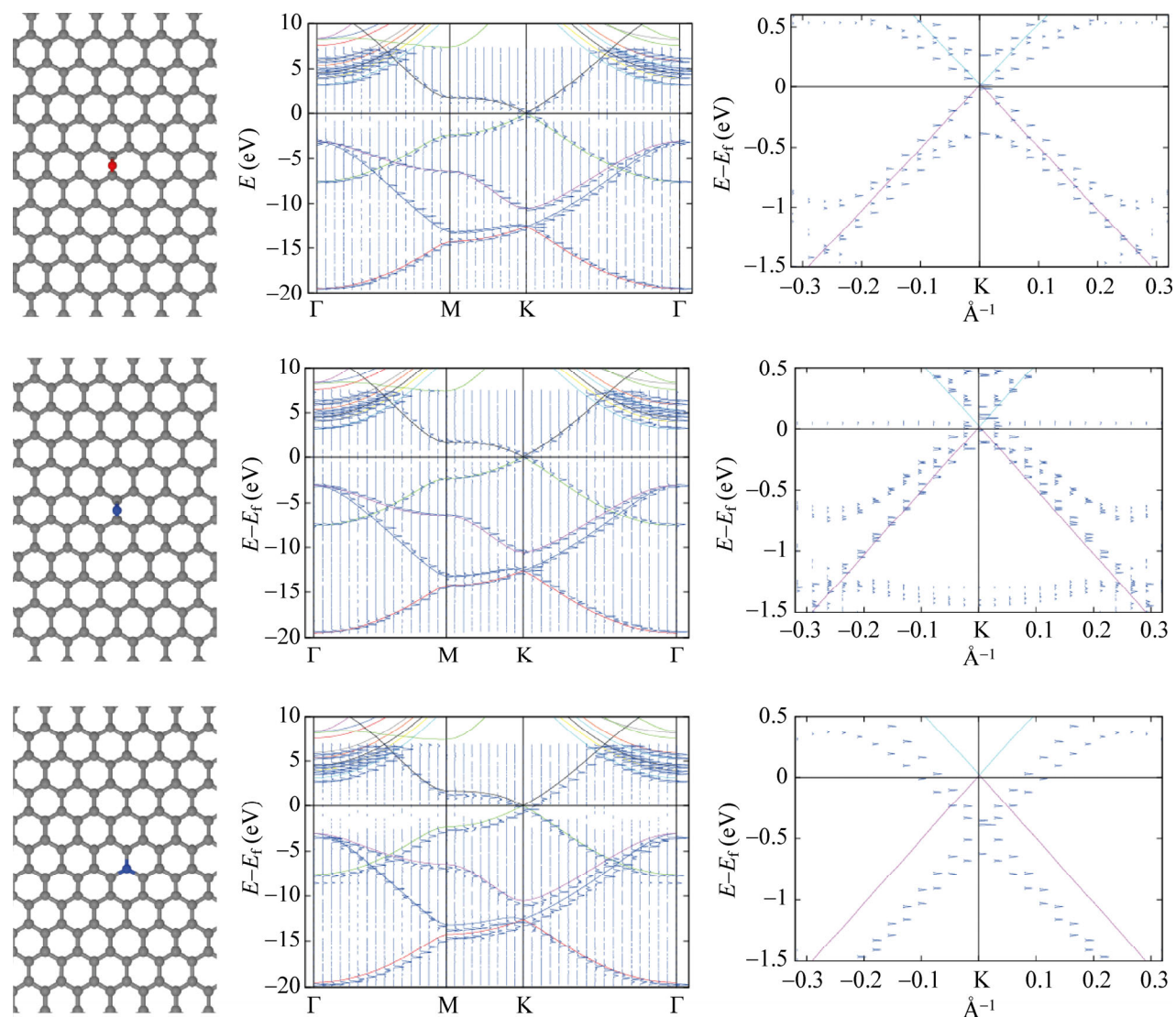


Figure S11 (Right) to (left) optimized structure, band structure, and magnified view of the band structure at the K point orthogonal to the Γ -K azimuth for, from (top) to (bottom), oxygen adatom, nitrogen adatom, and nitrogen substitution calculated using a 6×6 supercell. The band splitting introduced by the nitrogen substitution is due to the fact that only one of the two graphene sublattices is doped.

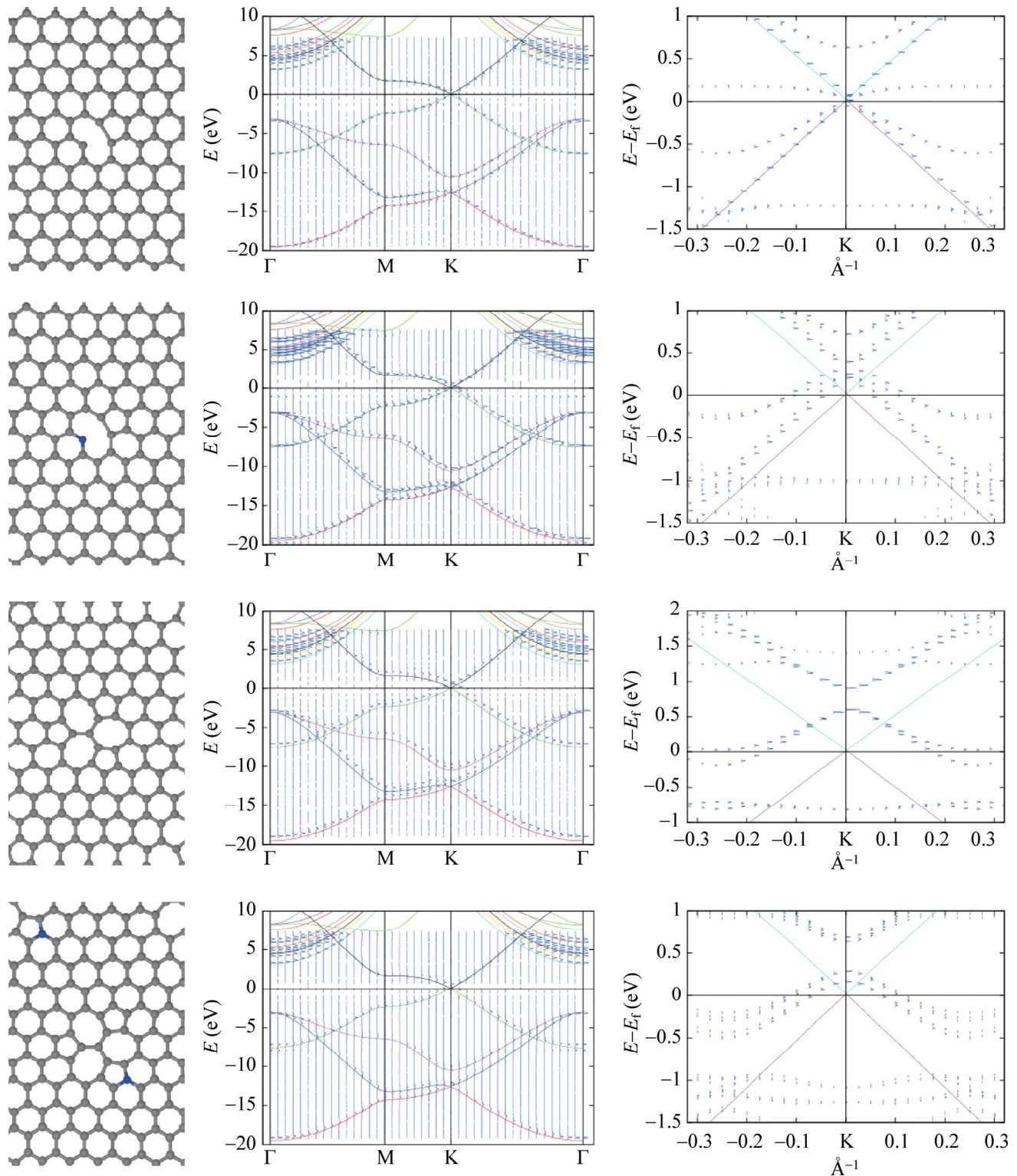


Figure S12 (Right) to (left) optimized structure, band structure, and magnified view of the band structure at the K point orthogonal to the Γ -K azimuth for, from (top) to (bottom), monovacancy, monovacancy with pyridinic nitrogen, 7,5,7,5,7,5 divacancy, and 7,5,7,5,7,5 divacancy with pyrrolic nitrogen calculated using a 6×6 supercell.

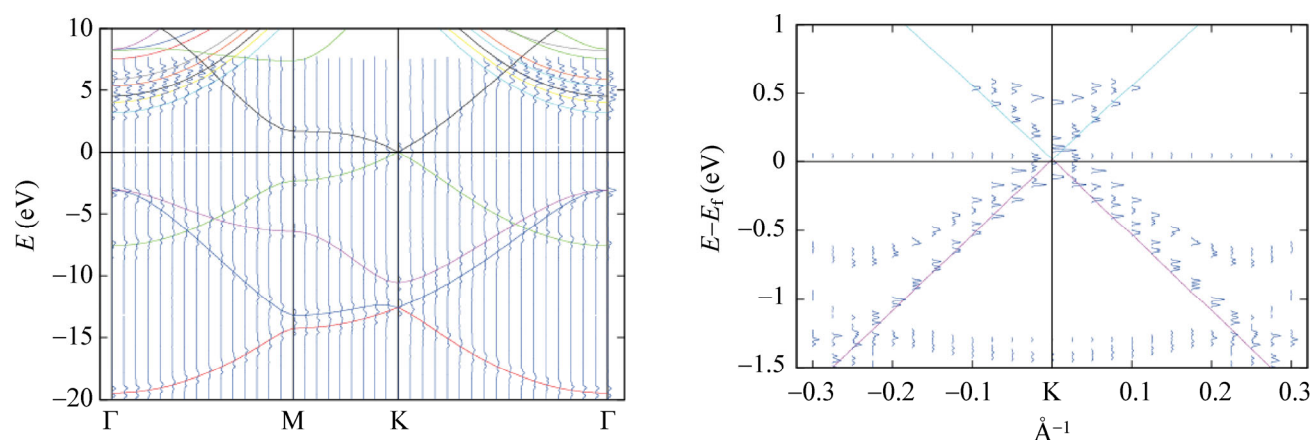


Figure S13 (Right) band structure, and (left) magnified view of the band structure at the K point orthogonal to the Γ -K azimuth for a weighted average of the defects considered as described above.

References

- [S1] Blume, R.; Kidambi, P. R.; Bayer, B. C.; Weatherup, R. S.; Wang, Z. J.; Weinberg, G.; Willinger, M. G.; Greiner, M.; Hofmann, S.; Knop-Gericke, A. et al. The influence of intercalated oxygen on the properties of graphene on polycrystalline Cu under various environmental conditions. *Phys. Chem. Chem. Phys.* **2014**, *16*, 25989–26003.
- [S2] Yang, D.; Velamakanni, A.; Bozoklu, G.; Park, S.; Stoller, M.; Piner, R. D.; Stankovich, S.; Jung, I.; Field, D. A.; Ventrice, C. A. et al. Chemical analysis of graphene oxide films after heat and chemical treatments by X-ray photoelectron and micro-Raman spectroscopy. *Carbon N. Y.* **2009**, *47*, 145–152.
- [S3] Hossain, M. Z.; Johns, J. E.; Bevan, K. H.; Karmel, H. J.; Liang, Y. T.; Yoshimoto, S.; Mukai, K.; Koitaya, T.; Yoshinobu, J.; Kawai, M. et al. Chemically homogeneous and thermally reversible oxidation of epitaxial graphene. *Nat. Chem.* **2012**, *4*, 305–309.
- [S4] Marsden, A. J.; Asensio, M. C.; Avila, J.; Dudin, P.; Barinov, A.; Moras, P.; Sheverdyeva, P. M.; White, T. W.; Maskery, I.; Costantini, G. et al. Is graphene on copper doped? *Phys. status solidi - Rapid Res. Lett.* **2013**, *7*, 643–646.
- [S5] Wilson, N. R.; Marsden, A. J.; Saghir, M.; Bromley, C. J.; Schaub, R.; Costantini, G.; White, T. W.; Partridge, C.; Barinov, A.; Dudin, P. et al. Weak mismatch epitaxy and structural feedback in graphene growth on copper foil. *Nano Res.* **2013**, *6*, 99–112.
- [S6] Brown, L.; Lochocki, E. B.; Avila, J.; Kim, C. J.; Ogawa, Y.; Havener, R. W.; Kim, D. K.; Monkman, E. J.; Shai, D. E.; Wei, H. I. et al. Polycrystalline graphene with single crystalline electronic structure. *Nano Lett.* **2014**, *14*, 5706–5711.
- [S7] Avila, J.; Razado, I.; Lorcy, S.; Fleurier, R.; Pichonat, E.; Vignaud, D.; Wallart, X.; Asensio, M. C. Exploring electronic structure of one-atom thick polycrystalline graphene films: A nano angle resolved photoemission study. *Sci. Rep.* **2013**, *3*, 2439.